Interaction between a Transition-Metal Fluoride and a Transition-Metal Hydride: Water-Mediated Hydrofluoric Acid Evolution Following Fluoride Solvation

UNIVERSITÀ DEGLI STUDI DI TORINO

Interaction between a transition metal fluoride and a transition metal hydride: water-mediated HF evolution following fluoride solvation.

Michele R. Chierotti,[a,b] Andrea Rossin,[c] Roberto Gobetto[a,c] and Maurizio Peruzzini*[c]*

[a] Dipartimento di Chimica, Università di Torino, V. Giuria 7, 10125 Torino, Italy. [b] NIS Centre of Excellence, Via Quarello 11, 10135 Torino, Italy. [c] Consiglio Nazionale delle Ricerche, Istituto di Chimica dei Composti Organometallici (ICCOM-CNR), Via Madonna del Piano 10, 50019 Sesto Fiorentino (Firenze), Italy.

KEYWORDS: Hydrogen bonding – nickel(II) – tungsten(II) – PCP pincer complexes – transition metal hydrides – transition metal fluorides – multinuclear NMR spectroscopy – reaction kinetics – DFT calculations.

ABSTRACT: The reaction between the nickel(II) PCP pincer fluoride complex (^{tBu}PCP)Ni(F) [^{tBu}PCP = 2,6-$C_6H_3(CH_2P^tBu_2)_2$] and the tungsten(II) carbonyl hydride $CpW(H)(CO)_3$ (Cp = η^5-$C_5H_5^-$) leads to hydrogen fluoride evolution and formation of the bimetallic isocarbonylic species [$CpW(CO)_2(\mu$-κC:κO-CO)···Ni(^{tBu}PCP)]. The process has been monitored through multinuclear (^{19}F, ^{31}P{^{1}H}, ^{1}H) variable-temperature NMR spectroscopy, collecting ^{19}F T_1 data values for a fluoride ligand bound to a transition metal. The extremely short relaxation time (minimum value of 13 msec at 193 K) is ascribed to the large chemical shift anisotropy of the Ni-F bond (688

ppm). The in-depth NMR analysis has revealed that the fluoride-hydride interaction is not direct but water-mediated, at odds with what was previously observed for the "hydride-hydride" case ($(^{tBu}PCP)Ni(H)$/ $CpW(H)(CO)_3$. Kinetic measurements have unveiled that the first step of the overall mechanism is thought to be the solvation of the fluoride ligand (as a result of a Ni-$F\cdots H_2O$ hydrogen bonding), while further reaction of the solvated fluoride with $CpW(H)(CO)_3$ is extremely slow, and competes with the side-reaction of fluoride replacement by a water molecule on the Ni centre to form the $[(^{tBu}PCP)Ni(H_2O)]^+$ *aquo* species. Finally, a DFT analysis of the solvation process through a discrete + continuum model has been accomplished, at the M06//6-31+G(d,p) level of theory, to support the mechanistic hypothesis.

Introduction.

Hydrogen bonding involving fluoride groups is one of the strongest directional, intermolecular and non-covalent interactions existing in chemistry.[1] The excellent ability of the fluoride ligand of forming hydrogen bonds with proton donors has been extensively documented in the inorganic chemistry literature,[2] where chemical evidences show that fluorides can act as hydrogen bond acceptors in $M–F^{\delta-}\cdots{}^{\delta+}HA$ interactions, exhibiting a Lewis basic character. Indeed, networks of hydrogen bonds are frequently detected in crystallographic studies of high valent metal fluorides when suitable proton donors such as the ammonium ion or water are present in the crystal lattice.[3] Most of the bi- and tervalent metal cations are able to form *aquo* complexes with water molecules as ligands; at the same time, these complexes contain fluorides either forming covalent M–F bonds with the metal center or being present as "independent" fluoride anions (*i.e.* not coordinated). Examples from the first group are the hydrated fluoride

salts $FeF_2 \cdot 4H_2O$,[4] $CuF_2 \cdot 2H_2O$,[5] or the mixed-metal species $CuZrF_6 \cdot 4H_2O$,[6] while compounds like $[Cr(H_2O)_6]F_3 \cdot 3H_2O$[7] belong to the second group. Comparison of the mean O–H···F hydrogen bond lengths exhibited by the above classes of fluoride hydrates clearly reveals the following trend: if the donor water molecules are engaged in an *aquo* complex, the hydrogen bond is strengthened, but engagement of the acceptor fluorine atoms in a complex anion (like ZrF_6^{2-}) weakens it. A number of structural studies of $L_nM–F\cdots H_2O$ hydrogen bonding (where M = transition metal; L = organic ligand) can be also found in the literature.[8] A special proton donor is hydrofluoric acid (HF): the reaction between HF and $L_nM–F$ often leads to formation of the bifluoride ligand $[F–H–F]^-$ on the metal centre. The most common synthetic methodology employed for the preparation of bifluoride complexes is the reaction between the corresponding hydrides or fluorides with $Et_3N\cdot(HF)_3$ ("TREAT HF"). The excess of HF favours the M–F···H–F hydrogen bond formation. At present, many examples of transition metal bifluoride complexes are known;[9] structural studies have unveiled the existence of both linear and bent HF_2^- coordination modes to metal ions. In addition, 1D and 3D coordination polymers showing M–F–H–F–M pillars/bridges could also be prepared, using pyrazine as bridging ancillary ligand.[10]

Recently, we have reported on the existence of an unconventional $M–H^{\delta-}\cdots{}^{\delta+}H–M'$ dihydrogen bonding between an acidic and a basic transition metal hydride,[11] along with the isolobal nature of the hydride and fluoride ligands in the pincer-type Ni(II) complexes ($(^{tBu}PCP)Ni(H)$ [**1**; $^{tBu}PCP = 2,6\text{-}C_6H_3(CH_2P^tBu_2)_2$] and $(^{tBu}PCP)Ni(F)$ (**2**).[12] The replacement of the hydride ligand in **1** with a (more electronegative) fluoride substituent increases the Ni–E (E = H, F) bond polarization considerably. The present study aims at getting a deeper knowledge on

the nature of the non-covalent interaction occurring between **2** and the acidic tungsten(II) hydride $CpW(H)(CO)_3$ (**3**; Cp = η^5-$C_5H_5^-$. Scheme 1), under the same experimental conditions employed for the "hydride-hydride" case.11 While "classical" hydrogen bonding between transition metal fluoride complexes and organic proton donors has already been reported in the literature,1,2 no examples of metal fluoride-metal hydride interactions have been studied at present (to the best of our knowledge). Multinuclear (^{19}F, $^{31}P\{^1H\}$, ^1H) variable-temperature NMR spectroscopy has been exploited as a powerful tool to gain insights into the interaction mechanism.[13] The direct involvement of water in the process leading to HF evolution is confirmed by the spectroscopic data. As a complement, DFT calculations were performed at the M06//6-31+G(d,p) level on a model system, following the methodology previously employed by some of us for the computational modelling of organometallics proton transfer reactions in aqueous media. [14]

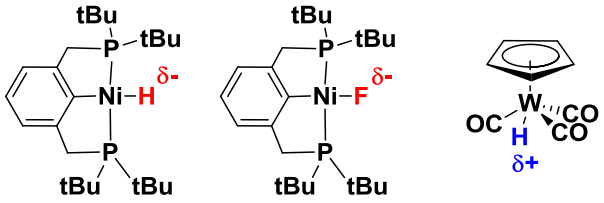

Scheme 1. The organometallics studied in this work.

Experimental Section

General Considerations. All reactions were performed using the standard Schlenk procedures under a dry nitrogen atmosphere, unless specified. All solvents employed were purged with nitrogen for 10 min. before use. (^{tBu}PCP)Ni(F) was prepared according to the literature procedure,12 while CpW(H)(CO)$_3$ (Aldrich) was purified by sublimation before use, and stored at –30 °C. Deuterated solvents (Aldrich) were degassed by three freeze-pump-thaw cycles before use.

Multinuclear (^{19}F, ^{31}P{^{1}H}, ^{1}H) variable-temperature solution NMR spectroscopy. ^{19}F, ^{31}P{^{1}H} and ^{1}H variable-temperature NMR spectra were recorded on a Jeol Eclipse+ 400 MHz spectrometer, equipped with a low-temperature measurement tool. Temperature calibration was carried out with a standard methanol ^{1}H thermometer. Referencing is relative to external TMS (^{1}H and ^{13}C), H_3PO_4 85% (^{31}P) and CCl_3F (^{19}F). Two-dimensional ^{1}H-NOESY and ^{19}F-^{1}H HOESY spectra were recorded on a Bruker DRX 400 MHz spectrometer with a mixing time of 800 and 75 msec, respectively.

Non selective inversion recovery was used to obtain ^{1}H T_1 values. Errors in the reported T_1 values were estimated to be in the range ± 2%.

Sample preparation: A THF-d_8 solution of **2** (1.5 equivalents) prepared in a Schlenk flask kept at 273 K (ice bath) was transferred *via* cannula into a 5 mm screwed-cap NMR tube containing a THF-d_8 solution of **3** stored at 195 K (dry ice/acetone bath). The samples were degassed using standard freeze/pump/thaw techniques and then transferred into the NMR spectrometer (kept at 190 K) and warmed stepwise to room temperature.

Solid-state NMR measurements. The ^{19}F MAS solid-state NMR spectrum of **2** was recorded on a Bruker 400 Avance II operating at 376.59 for ^{19}F. A cylindrical 2.5 mm o.d. zirconia rotor with a sample volume of 12 mL was employed and spun at 28 kHz at RT. A direct excitation

experiment was used with a ^{19}F 90° pulse of 5.35 μsec and a relaxation delay of 1 s for 512 scans. The ^{19}F scale was referenced with the resonance of external solid Polytetrafluoroethylene (Teflon).

Kinetic measurements. The variation of the concentration of **2** during the reaction with **3** was monitored at 273 K through the integration of the related $^{31}P\{^1H\}$ NMR signal, in both pure THF (freshly distilled from sodium-benzophenone under N_2) and in THF/water binary mixtures at different water molarity ranging between 0.1 and 1.3 M (corresponding to a 1 : 1 : 1 and a 1 : 1 : 20 relative **2** : **3** : H_2O stoichiometric ratio, respectively). A coaxial external standard of a toluene-d_8 triphenylphospine oxide solution (0.23 M, δ_P = 27.7 ppm, singlet) was employed, to have a reference signal for the peaks integration. $^{31}P\{^1H\}$ NMR spectra were recorded on a BRUKER AVANCE II 300 MHz spectrometer; $^{31}P\{^1H\}$ was referenced to 85% H_3PO_4 with downfield shift taken as positive.

Computational Details. Density Functional Theory (DFT) calculations were performed using the *Gaussian09* program (revision *A.02*).[15] Model structures were optimized with a M06 functional[16] (already employed successfully in other cases for the treatment of non-covalent bonds[17]) using the SDD (Ni, W)[18]/D95 (P)[19] pseudopotentials and related basis sets on the Nickel, Tungsten and Phosphorus atoms, a 6-31G* basis on Carbon, Oxygen and the pincer protons and a more extended 6-31+G(d,p) basis on the fluoride/hydride ligands and the water protons. Introduction of diffuse functions is essential to well-reproduce conformational equilibria and experimental electron affinities.[20] An extra *d*-type polarization function for P and an extra *f*-type function for Ni and W were added to the standard set.[21] Gibbs energy calculations to infer relative thermodynamic stabilities were carried out on a *model* system, with the *tert*-butyl groups on the pincer ligand replaced by H atoms (^{H}PCP). The model compound (^{H}PCP)Ni(F) (**2^{H}**) was

therefore used in the simulations. A *discrete-continuum* modelling of the reaction medium was employed. A cluster made of four water molecules $(H_2O)_4$ was explicitly included in the model, and the internal energies were evaluated in a water/THF solution where the molar fraction of water was assumed to be 0.1 (approximately corresponding to a 1.3 M concentration), represented as a polarizable continuum medium (SMD, $\varepsilon = 10.09$)[22,23] with the same basis set used for the gas phase optimizations, following the methodology recently employed by some of us for DFT studies of organometallic hydrides reactivity in aqueous solutions. This cluster size was previously found to be the optimal compromise between a realistic system description and reasonably short computational times.14,[24] Gibbs energy in solution was calculated according to the simplified equation:

$$G_{solv} = G_{gas} + (E_{solv} - E_{gas})$$

For the transition state $\mathbf{TS_1}$ analytical frequencies were calculated, to check that only one imaginary value is obtained, related to a saddle point on the Potential Energy Surface. Normal coordinate analyses on these stationary points were also performed by intrinsic reaction coordinate (IRC) calculations[25] in both directions to the correspondent minima. When the IRC calculations failed to reach the minima, geometry optimizations from the initial phase of the IRC path were performed.

Results and Discussion

(a) Multinuclear variable-temperature NMR experiments. Equimolar amounts of **2** and **3** were mixed in carefully degassed THF-d_8 at 193 K under a nitrogen atmosphere. A slow temperature increase to 298 K led to a dark-orange solution, from which a reddish-orange

crystalline material precipitated, with concomitant HF formation. NMR analysis revealed that the final product is the same obtained from the reaction of the analogous hydride compound **1**, the bimetallic compound **4**. Here, we would like to demonstrate that the **2-3** interaction, in spite of generating the same final product, takes place through a different mechanism. As already reported, the **1-3** reaction implies the formation of a **1···3** adduct through an Ni–H···H–W direct interaction.11 On the contrary, in the case of the fluoride **2**, the reaction seems to proceed through the formation of a putative **2···H_2O···3** adduct (Scheme 2), as a consequence of the (unavoidable) presence of water coming from the synthesis of **2**.[26]

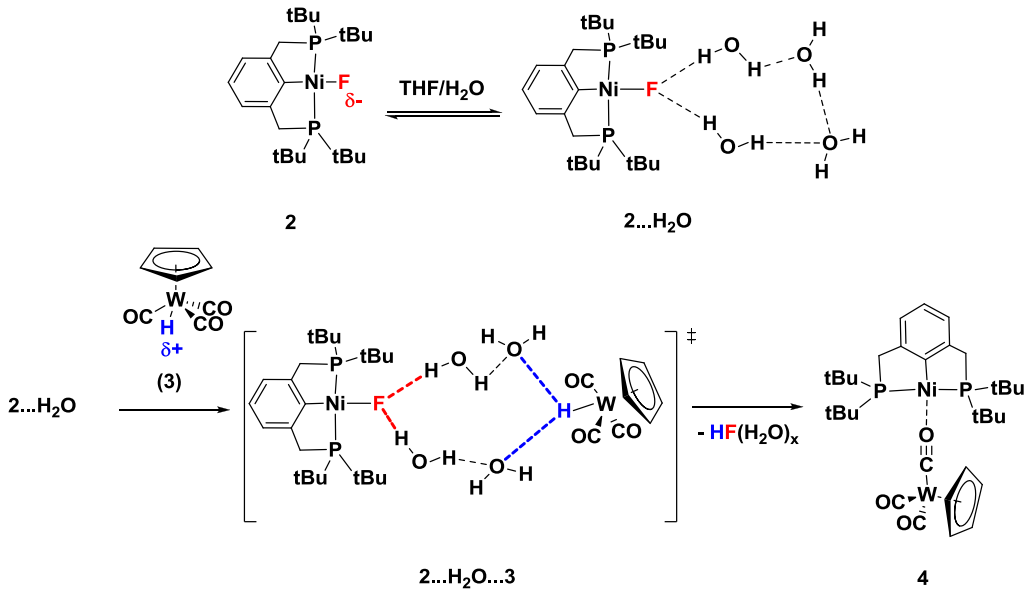

Scheme 2. Water-assisted HF evolution from the **2-3** interaction.

In order to cast light on the reaction mechanism, a thorough NMR analysis that combines a multinuclear and multiparametric variable temperature (VT) approach (^{1}H, ^{19}F, ^{31}P{^{1}H}, ^{1}H NOESY, ^{19}F-^{1}H HOESY, ^{1}H and ^{19}F T_1 relaxation measurements) was performed. All ^{1}H, ^{19}F

and $^{31}P\{^{1}H\}$ NMR chemical shifts (δ) with assignments for reagents, intermediate and product are listed in Table S1. Table S2 reports the ^{1}H NMR chemical shifts, together with $T_1(^{1}H)$ relaxation values at different temperatures, while Table S3 is the same data collection for ^{19}F. The ^{1}H NMR spectrum of pure **3** in THF-d_8 at 293 K (Figure S1) is characterized by the Cp and WH resonances at 5.63 and −7.37 ppm, respectively. In both pure **3** and **2···H_2O···3**, the hydride resonance at −7.37 ppm slightly shifts towards lower frequencies by decreasing the temperature, but both scalar coupling and line width do not change (Figure S2 and Table S2).

No hydride shift is observed upon **2···H_2O···3** formation, although a substantial change in the hydride relaxation time occurs (*vide infra*). This indicates the formation of a weak interaction involving the hydride ligand (NOESY and HOESY experiments will clarify the role of the water in the interaction, see below). The lack of signal shift agrees with the limited amount of **2···H_2O···3** formed and the small shift of only 0.04 ppm for direct Ni-H…H-W interaction previously found.[11]

The ^{19}F signal at −372.6 ppm of pure **2** undergoes a significant high frequency shift (1.5 ppm) when equimolar amounts of **3** are added (Table S3). It is also worth noticing that a large increase of the ^{19}F linewidth was observed for pure **2** (Figure S3) and for **2···H_2O···3** (Figure 1) on decreasing the temperature, preventing the direct measurement of the fluorine-hydrogen coupling constants. This behavior is explained in terms of very short ^{19}F T_2 values in agreement with the extremely short T_1 values (see below).

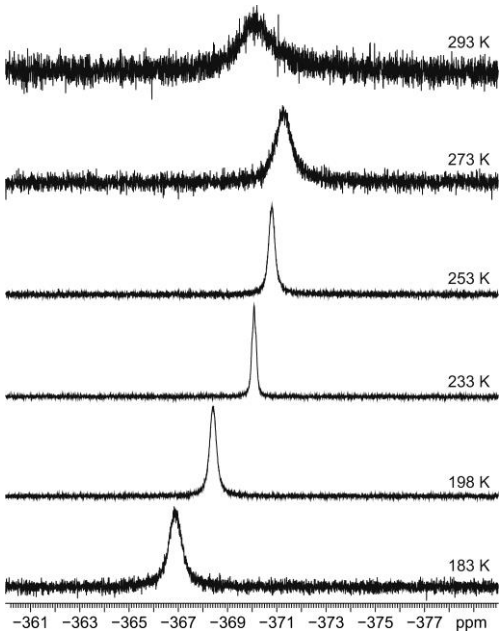

Figure 1. VT ^{19}F (376.59 MHz) NMR spectra (THF-d_8) of **2**···**H_2O**···**3**.

After leaving the solution at 263 K for 3-4 hours, the doublet assigned to solvated HF [*i.e.* (HF) · $(H_2O)_n$] started appearing on both ^{1}H and ^{19}F NMR spectra (^{1}H δ = 11.64 ppm and ^{19}F δ = −184.7 ppm, $^1J_{HF}$= 422 Hz; Figure S4), in agreement with the formation of **4** with HF evolution. At odds with other literature cases,9 no Ni–FHF bifluoride complex formation was observed: only *one sharp* ^{19}F NMR doublet is recorded (Figure S4). This can be justified by the very small amount of HF present in solution at all times and temperatures [the reaction leading to **4** and HF is extremely slow, as evidenced by the kinetic studies reported in section (c)]. Bifluoride complexes normally form from organometallic fluorides under an *excess* of HF.

Informative results came from the analysis of both ^{1}H NOESY and ^{19}F-^{1}H HOESY experiments. The ^{1}H NOESY spectrum of **2**···**H_2O**···**3** collected at 263 K only shows intramolecular noesy cross peaks (red signals in Figure 2) between ^{t}Bu and Cp protons, in

agreement with the formation of the adduct as well as with the theoretical calculations (*vide infra*). Other intramolecular correlations are observed between the CH_2/^{t}Bu (3.06/1.43 ppm), the phenyl/CH_2 (6.64/3.06 ppm), the phenyl/^{t}Bu (6.64/1.43 ppm) and the hydride/Cp (–7.38/5.71 ppm, not visible in the Figure) protons. An exchange process was also found between H_2O and the hydride **3** protons (2.80/–7.38 ppm, blue cross peaks in Figure 2). However, no H_2O/**3** exsy cross peaks were observed when recording the ^{1}H NOESY experiment (even with several mixing times) of pure **3**. The latter finding is in line with the outcome of the theoretical analysis (*vide infra*), which confirms the absence of strong interactions of water with the W–H bond in **3**. From a purely experimental point of view, the *aquo* complex formation is not observed in the case of a wet THF solution of pure **3**, the hydride being rather inert towards water.

Interestingly, the ^{1}H NOESY spectrum of the analogous **1**···**3** adduct (acquired under the same experimental conditions) did not show any exsy cross peaks.

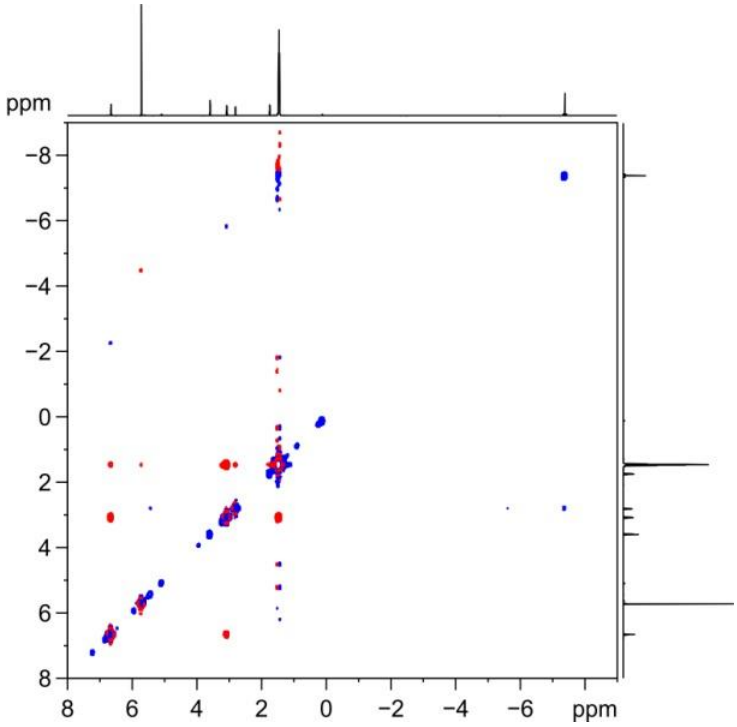

Figure 2. ^{1}H (400.23 MHz) NOESY spectrum (THF-d_8) of **2**···**H_2O**···**3** recorded at 263 K with a mixing time of 0.8 sec. Red negative and blue positive signals represent noesy and exsy correlations, respectively.

This indicates that the reaction mechanism is different and it is related to the type of substituent on the Ni centre, *i.e.* hydride or fluoride. In this sense, the polarization of the Ni–F bond plays a fundamental role in activating solvation phenomena through the formation of Ni–F···H_2O hydrogen bonds which have a deep influence on the mechanism of the Ni-W interaction. As an additional proof of evidence, the ^{19}F-^{1}H HOESY spectrum collected at T = 243 K (Figure 3) is characterized by the noesy **2**/H_2O cross peak and by the lack of noesy cross peaks between fluoride and hydride signals. This definitely highlights the water role in assisting and mediating the **2**-**3** interaction.

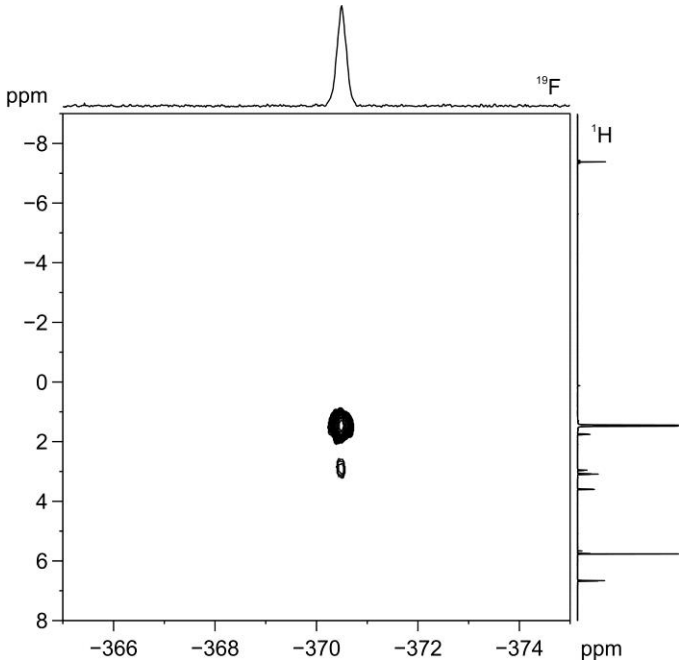

Figure 3. ^{19}F-^{1}H HOESY NMR spectrum (THF-d_8) of **2**···**H_2O**···**3** recorded at 243 K with a mixing time of 75 msec. Noesy peaks are observed for F/^{t}Bu (-371.4/1.45 ppm) and F/H_2O (-371.4/2.95 ppm).

(b) T_1 relaxation analysis. ^{19}F T_1 of pure **2** is only 97 msec at 293 K. This value decreases on lowering the temperature, reaching a minimum value of 13 msec between 193 and 183 K and then slowly increasing to 16 msec at 173 K. EPR measurements ruled out the presence of paramagnetic impurities responsible for the extremely short T_1 values. At the same time, the small relaxation times cannot be ascribed to the dipolar contribution (which would justify these values only in the presence of very short F···F or F···H interactions; the existence of these contacts is ruled out by the NOESY and HOESY experiments). Moreover, there is no dependence of T_1 from the sample concentration, thus excluding any phenomenon of molecule aggregation in solution. Therefore, the very short ^{19}F T_1 values can be ascribed to the chemical shift anisotropy (CSA) mechanism, according to Equation 1:

$$\frac{1}{T_1} = \frac{2}{15}\left(\sigma_{//} - \sigma_{\perp}\right)^2 {\omega_F}^2 \tau_c \frac{1}{\left(1 + {\omega_F}^2 {\tau_c}^2\right)} \qquad (1)$$

where $\sigma_{//}$ and $\sigma_{\perp}$ are referred to the parallel and perpendicular shielding with respect to the magnetic field, respectively, τ_c is the correlation time and ω_F the fluorine Larmor frequency.

The fast ^{19}F relaxation is triggered by the high gyromagnetic ratio and CSA, although the known literature values for fluorine anisotropy are mostly referred to C–F bonds in organic compounds and therefore they are rather limited.[27] Equation 1 has a minimum when $\omega_F\tau_c$ =0.62,

then the experimental T_1 value measured at 193 K provides a value for the ^{19}F chemical shift anisotropy of about 688 ppm. This value is the largest ever recorded for ^{19}F anisotropy, but also the only one, to our knowledge, referring to an M-F interaction with M being a transition metal. On the other hand, a large CSA value is expected, since the ^{19}F chemical shift of **2** (approximately –370 ppm; it represents the isotropic value of the three components of the shielding tensor) is quite far away from the commonly found ^{19}F NMR chemical shift range. Thus, the ^{19}F MAS solid-state NMR spectrum of **2** has been recorded (Figure S4). In addition to the isotropic peak, an extended pattern of spinning sidebands associated to a chemical shift anisotropy of about 663±20 ppm (span value, following the Herzfeld-Berger convention[28]) can be clearly seen, in good agreement with the anisotropy value calculated in solution. Very short ^{19}F T_1 values preclude the possibility to use the ^{19}F relaxation times to confirm the formation of **2**···$\mathbf{H_2O}$ or **2**···**3** interactions, because the contribution of the heteronuclear dipolar mechanism is negligible if compared with the much more efficient CSA mechanism. In line with this statement, the ^{19}F T_1 values are almost identical for pure **2** and for **2**···$\mathbf{H_2O}$···**3**. Interestingly, the ^{19}F signal linewidth increases when decreasing the temperature; this is due to the very short T_2 values related to the high CSA contribution to spin-spin relaxation, according to Equation 2.

$$\frac{1}{T_2} = \frac{2}{15}\left(\sigma_{//} - \sigma_{\perp}\right)^2 \omega_F{}^2 \tau_c \left(\frac{2}{3} + \frac{1}{2}\frac{1}{\left(1 + \omega_F{}^2 \tau_c{}^2\right)} \right) \qquad (2)$$

Conversely, ^1H T_1 values of the hydride resonance of **3** showed a remarkable decrease when equimolar amounts of **2** were added to the solution, passing (for example) from 7.2 to 5.8 sec at

198 K. This suggests that an additional contribution to the ^1H T_1 due to dipole-dipole intermolecular interaction with the Ni-F-water cluster may be present, according to Equation 3:

$$\frac{1}{T_1} = \frac{3}{10}\left(\frac{\mu_0}{4\pi}\right)\frac{\gamma_H{}^4\hbar^2}{r_{HH}{}^6}\,\tau_c\left(\frac{1}{\left(1+\omega_H{}^2\tau_c{}^2\right)}+\frac{4}{\left(1+4\omega_H{}^2\tau_c{}^2\right)}\right) \qquad (3)$$

γ_H is the ^1H gyromagnetic ratio, h is the Boltzmann Constant, and r_{HH} is the internuclear H---H distance and ω_H the proton Larmor frequency.

(c) Kinetic studies: formation of the *aquo* complex [(^{tBu}PCP)Ni(H$_2$O)]$^+$. The role of water in the reaction between **2** and **3** evidenced by the NOESY and HOESY NMR spectra has been further analyzed through kinetic measurements of the reaction rate through $^{31}P\{^1H\}$ NMR signal integration in the presence of an external standard. Experiments were performed at 273 K with different THF/water mixtures (water molarity ranging between 0.1 M and 1.3 M). While monitoring –d[(^{tBu}PCP)Ni(F)]/d*t* in wet THF (1.3 M in H_2O), within the first 13 minutes (*ca.* 800 sec) a significant decrease of the fluoride concentration was recorded (Figure 4). This is surely related to the replacement of the fluoride ligand by an *aquo* ligand on Ni(II) coordination sphere, with concomitant formation of [(^{tBu}PCP)Ni(H$_2$O)]$^+$ (**5**) and the solvated fluoride anion [F(H$_2$O)$_x$]$^-$ (as an ion pair).

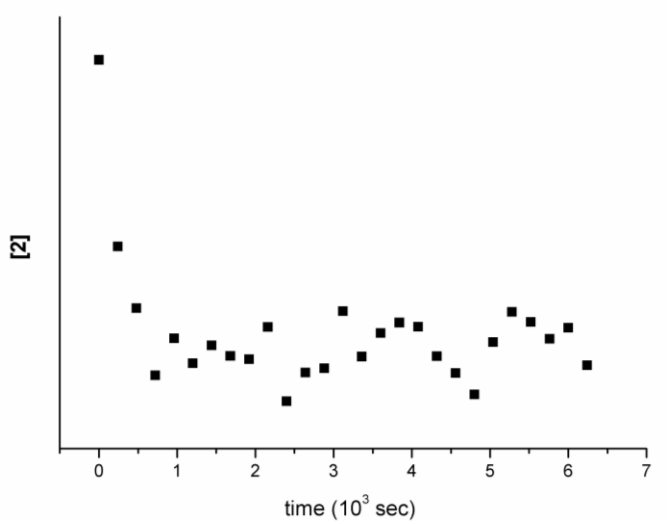

Figure 4. Variation of [**2**] in time in a **2**···**H_2O**···**3** wet THF solution {T = 273 K, [H_2O] = 1.3 M, (**2** : **3** : **H_2O**) stoichiometric ratio = (1 : 1 : 20)}. The Y-axis values are inferred from the $^{31}P\{^1H\}$ NMR signal integration of the characteristic doublet of **2** with respect to an external triphenylphospine oxide standard at known and constant concentration (see Experimental Section).

In line with this hypothesis, a new $^{31}P\{^1H\}$ NMR signal at δ_P = 74.4 ppm and growing with time started to appear together with that of **4** (Figure S6). This signal had been previously assigned to the cation **5**, by adding water to pure **2** in THF in an independent experiment.[29] From all these results, it can be stated that water acts as a competitive reagent towards **2**, and the higher its concentration the slower will be the formation of **4**. Evolution to the bimetallic product is severely hampered by the solvation sphere created by water around the F^- ligand. At this stage, the reaction rate becomes extremely slow, and the concentration of **2** is practically constant in time (since its consumption is too slow to be measured accurately in a reasonable time scale;

only a negligible statistical deviation of the collected kinetic data points from a mean constant value is recorded, Figure 4). Therefore, it is impossible to propose any meaningful kinetic law for the formation of **4**.

(d) DFT modeling of the solvation process. The interaction of water with **2** and **3** has been further analyzed from a computational point of view, at the M06//6-31+G(d,p) level of theory. To this aim, a simplified structure for **2** was taken into account for the calculations, where the bulky *tert*-butyl groups were replaced with hydrogen atoms, to achieve the best compromise between model system accuracy and computational time. The resulting (^{H}PCP)Ni(F) complex ($\mathbf{2^H}$) was assumed to be the starting reagent. Initially, the direct interaction between $\mathbf{2^H}$ and **3** has been simulated; at odds with what was found in the "hydride-hydride" Ni–H···H–W case,11 in the optimized model structure no Ni–F···H–W hydrogen bonding is found. A preferential Ni-F···H-C(Cp) interaction involving the (more acidic) Cp protons is instead observed [optimized d(Ni–F···H–C) = 1.92 Å, $\mathbf{2^H\cdots 3}$, Figure S7]. The calculated Mulliken charges on the fluoride ligand and on the interacting Cp proton are indeed the highest of the whole system (q_F = –0.5 e; q_H = +0.3 e). At the same time, a weak Ni···H–W interaction is also present [optimized d(Ni···H–W) = 2.47 Å]. Both atoms are electronically neutral (Mulliken charges: q_{Ni} = +0.08 e; q_H = +0.05 e). Therefore, HF evolution must take place through a different type of mechanism (*i.e.* it must be solvent-mediated), this hypothesis being perfectly in line with the experimental results.

Before putting the two reagents together in the computation, the interaction of $(H_2O)_4$ with $\mathbf{2^H}$ and **3** was examined separately; while $\mathbf{2^H}$ engages in a double Ni–F···HOH hydrogen bonding [optimized d(Ni–F···HOH) = 1.72 and 1.80 Å, $\mathbf{2^H\cdots(H_2O)}$, Figure S8], **3** does not form any kind

of hydrogen bonding through its hydride substituent [shortest d(W–H···OH_2) = 2.52 Å]. A preferential interaction with the *carbonyl ligands and the Cp protons* occurs instead [optimized d(C≡O···HOH) = 1.90 and 2.08 Å; shortest contact Cp–H···OH_2 = 2.37 Å, **3···(H_2O)**, Figure S9]. In line with the NMR analysis, the presence of a very small Mulliken charge on the hydride (calculated q_H = +0.06 e) makes the interaction of water with the CO or Cp ligands more favorite than that with the hydride substituent itself. The weak hydrogen bonding ability of the W–H bond in **3** towards organic bases (phosphine oxides, amines, pyridine) had already been pointed out in previous spectroscopic and computational studies.[30]

After this preliminary investigation, **2^H···(H_2O)** was combined with the (pre)-optimized geometry of **3**, and the ensemble was re-optimized again; the resulting **2^H···(H_2O)···3** adduct is shown on Figure 5. The water cluster is now bridging the hydride and the fluoride complexes through a complex H-bonding network. The shortest W–H···OH_2 distance is 2.78 Å, and weak Cp–H···OH_2 and C≡O···HOH interactions are present as seen in **2^H···(H_2O)** (distances equal to 2.39 and 2.18 Å, respectively).

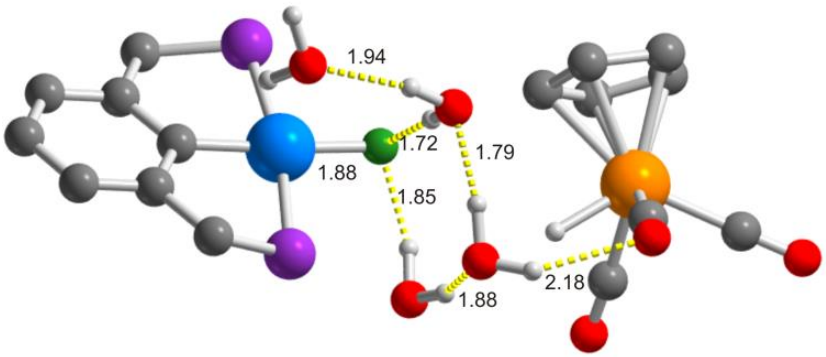

Figure 5. Optimized geometry of (^{H}PCP)Ni(F)···(H_2O)$_4$···CpW(H)(CO)$_3$ [**2^H···(H_2O)···3**]. Selected optimized bond lengths reported (Å). Hydrogen bonds depicted with yellow dotted

lines. H atoms on the organic ligands of both complexes omitted for clarity. Atom color code: white, H; gray, C; purple, P; blue, Ni; orange, W; green, F; red, O.

HF formation is probably induced by an indirect mechanism, where the water bridge acts as a "proton shuttle" between **2** and **3**; this kind of process was also invoked in the case of proton transfer reactions for water-soluble organometallic hydrides.14 A Potential Energy Surface (PES) scan along the d(W–H···OH_2) reaction coordinate was performed; a Transition State $\mathbf{TS_1}$ (Figure 6) lying at 9.5 kcal mol^{-1} above the reagent leads to an intermediate structure where the proton coming from the W–H bond dissociation is "hosted" by the water cluster: (^{H}PCP)Ni(F)···$(H_2O)_3(H_3O)^+$···$CpW(CO)_3^-$ ($\mathbf{6^H}$, Figure 7). The ΔG for the $\mathbf{2^H\cdots(H_2O)\cdots 3 \rightarrow 6^H}$ transformation equals +5.8 kcal mol^{-1}.

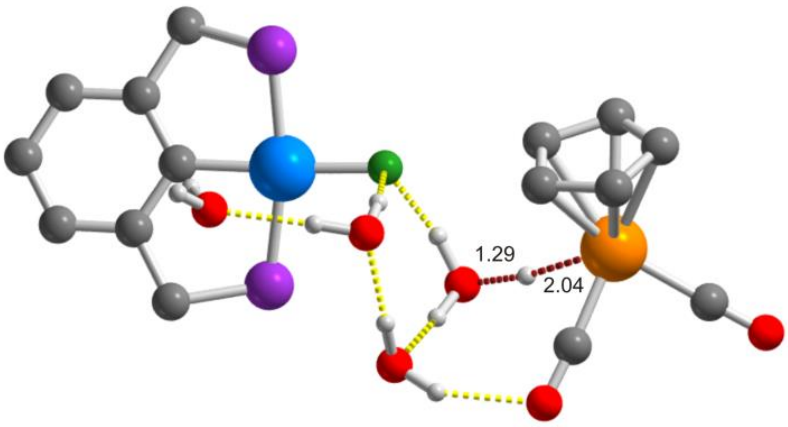

Figure 6. Optimized geometry of $\mathbf{TS_1}$. Selected optimized bond lengths reported (Å). Bonds directly related to the Transition State transformation drawn in brown dotted lines. Hydrogen bonds depicted with yellow dotted lines. H atoms on the organic ligands of both complexes omitted for clarity. Atom color code: see Figure 5.

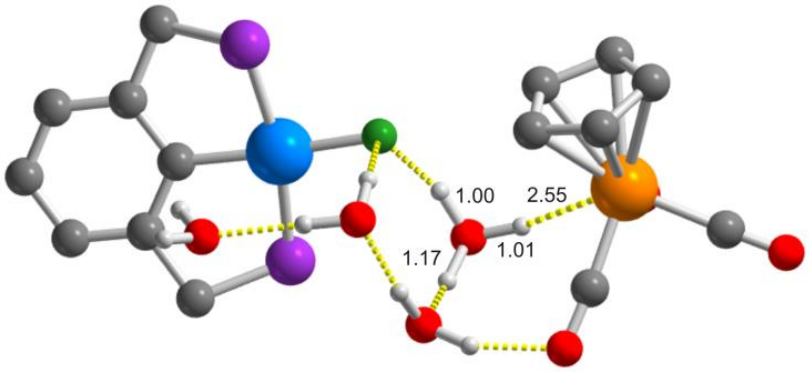

Figure 7. Optimized geometry of (^{H}PCP)Ni(F)···$(H_2O)_3(H_3O)^+$···$CpW(CO)_3^-$ (**6^{H}**). Selected optimized bond lengths reported (Å). Hydrogen bonds depicted with yellow dotted lines. H atoms on the pincer ligand and on the Cp ring omitted for clarity. Atom color code: see Figure 5.

From **6^{H}**, fluoride dissociation and concomitant *aquo* complex/HF formation lead to the final structure [(^{H}PCP)Ni(H_2O)][$CpW(CO)_3$]···[(HF)$(H_2O)_3$] (**7^{H}**, Figure 8). An approximate value of the activation barrier for this step is 4.3 kcal mol^{-1}.[31] Thermodynamics is almost thermoneutral for HF formation: the ΔG for the **2^{H}···(H_2O)···3** → **7^{H}** conversion equals –0.5 kcal mol^{-1}. Thus, the higher energy barrier to overcome in order to achieve HF formation under these conditions is around 10 kcal mol^{-1}, small enough for the reaction to occur at ambient temperature.

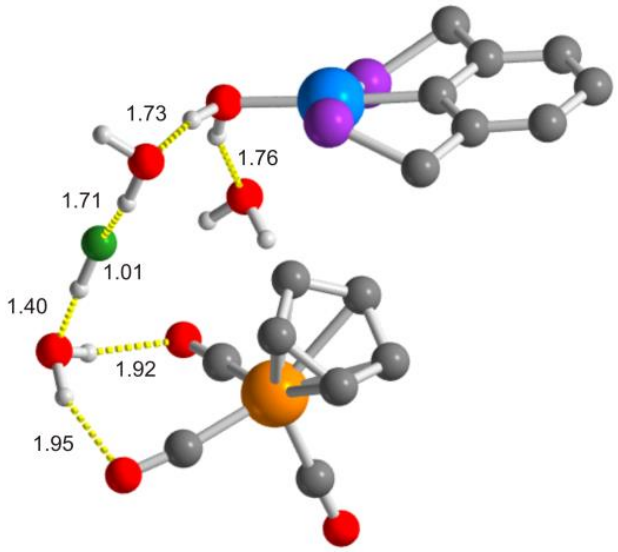

Figure 8. Optimized geometry of [(^{H}PCP)Ni(H_2O)] [$CpW(CO)_3$]···[$HF(H_2O)_3$] (**7^{H}**). Selected optimized bond lengths reported (Å). Hydrogen bonds depicted with yellow dotted lines. H atoms on the pincer ligand and on the Cp ring omitted for clarity. Atom color code: see Figure 5.

Conclusions.

The interaction between a transition metal fluoride and a transition metal hydride that leads to HF generation has been described; the reaction follows a different mechanistic path with respect to the analogous "hydride-hydride" case. No direct hydride-fluoride reaction takes place; the presence of water is of fundamental importance for the reaction progress, and a water-assisted process may be invoked, through the solvation of the fluoride ion followed by a Grotthuss-like proton transfer[32] mediated by a protonated water cluster. Multinuclear VT-NMR spectroscopy and DFT simulations on model compounds have been proved to be extremely efficient and complementary tools for an accurate analysis of this class of processes.

Associated Content

Supporting Information. Tables S1-S3, Figures S1-S9. Cartesian xyz coordinates and (selected) absolute G_{solv} energy values of $\mathbf{2^H\cdots 3}$, $\mathbf{2^H\cdots(H_2O)}$, $\mathbf{3\cdots(H_2O)}$, $\mathbf{2^H\cdots(H_2O)\cdots 3}$, $\mathbf{TS_1}$, $\mathbf{6^H}$ and $\mathbf{7^H}$. This material is available free of charge via the Internet at http://pubs.acs.org.

Author Information

Corresponding Author : * maurizio.peruzzini@iccom.cnr.it

Acknowledgments

The PIRODE project of the Italian Ministry of the Environment (MATTM), the EFOR and "Premiale 2011" projects of the Italian National Research Council are acknowledged for financial support. The use of the computational facilities of the Centre de Serveis Científics i Acadèmics de Catalunya (CESCA) is greatly appreciated. Thanks are also given to the FIRENZE HYDROLAB 2 project supported by ECRF. Mr. Fabrizio Zanobini and Mr. Andrea Rossi (ICCOM-CNR) are acknowledged for help with the preparation of **2** and for running the kinetic measurements. Authors are indebted with Prof. A. Macchioni and Dr. C. Zuccaccia (University of Perugia, Italy) for the use of the NMR facilities in their lab and for stimulating discussions.

References

(1) (a) Steiner, T.; *Angew. Chem. Int. Ed.* **2002**, *41*, 48. (b) Brammer, L.; Bruton, E. A.; Sherwood, P. *Cryst. Growth. Des.* **2001**, *1*, 277; (c) Desiraju, G. R.; Steiner, T. *The Weak*

Hydrogen Bond; Oxford University Press: Oxford, 1999. (d) Richmond, T. G. *Coord. Chem. Rev.* **1990**, *105*, 221, and references therein.

(2) (a) Martinez-Prieto, L. M.; Melero, C.; del Rio, D.; Palma, P.; Campora, J.; Alvarez, E. *Organometallics* **2012**, *31*, 1425. (b) Clot, E.; Eisenstein, O.; Jasim, N.; McGregor, S. A.; McGrady, J. E.; Perutz, R. N. *Acc. Chem. Res.* **2011**, *44*, 333. (c) Dransfield, T. A.; Nazir, R.; Perutz, R. N.; Whitwood, A. C. *J. Fluorine Chem.* **2010**, *131*, 1213. (d) Libri, S.; Jasim, N. A.; Perutz, R. N.; Brammer, L. *J. Am. Chem. Soc.* **2008**, *130*, 7842. (e) Murphy, V. J.; Hascall, T.; Chen, J. Y.; Parkin, G. *J. Am. Chem. Soc.* **1996**, *118*, 7428. (f) Peris, E.; Lee, J. C.; Rambo, J. R.; Eisenstein, O.; Crabtree, R. H. *J. Am. Chem. Soc.* **1995**, *117*, 3485.

(3) Babel, D.; Massa, W. *Chem. Rev.* **1988**, *88*, 275.

(4) Penfold, B. R.; Taylor, M. R. *Acta Crystallogr.* **1960**, *13*, 953.

(5) Prince, E. *J. Chem. Phys.* **1972**, *56*, 4352.

(6) Fischer, J.; Weiss, R. *Acta Crystallogr.* **1973**, *B29*, 1955.

(7) Epple, M.; Massa, W. *Z. Anorg. Allg. Chem.* **1978**, *444*, 47.

(8) (a) Lian, Z.; Xu, X; Sun, H.; Chen, Y.; Zheng, T.; Li, X. *Dalton Trans.* **2010**, *39*, 9523. (b) Fawcett, J.; Harding, D. A. J.; Hope, E. G.; Singh, K.; Solan, G. A. *Dalton Trans.* **2009**, 6861. (c) Schaub, T.; Fischer, P.; Steffen, A.; Braun, T.; Radius, U.; Mix, A. *J. Am. Chem. Soc.* **2008**, *130*, 9304. (d) Miyamoto, R.; Hamazawa, R. T.; Hirotsu, M.; Nishioka, T.; Kinoshita, I.; Wright, L. J. *Chem. Commun.* **2005**, 4047 (e) Jasim, N. A.; Perutz, R. N.; Whitwood, A. C.; Braun, T.; Izundu, J.; Neumann, B.; Rothfeld, S.; Stammler, H.-G. *Organometallics* **2004**, *23*, 6140.

(9) Pd–FHF: (a) Grushin, V. V. *Acc. Chem. Res.* **2010**, *43*, 160. (b) Ball, N. D.; Sanford, M. S. *J. Am. Chem. Soc.* **2009**, *131*, 3796. (c) Roe, D. C.; Marshall, W. J.; Davidson, F.; Soper, P. D.; Grushin, V. V. *Organometallics* **2000**, *19*, 4575. (d) Pilon, M. C.; Grushin, V. V. *Organometallics* **1998**, *17*, 1774. Rh–FHF: Segarra, C.; Mas-Marzá, E.; Lowe, J. P.; Mahon, M. F.; Poulten, R. C.; Whittlesey, M. K. *Organometallics* **2012**, *31*, 8584. Ru–FHF: Jasim, N. A.; Perutz, R. N.; Foxon, S. P.; Walton, P. H. *J. Chem. Soc., Dalton Trans.* **2001**, 1676. Pt–FHF: Jasim, N. A.; Perutz, R. N. *J. Am. Chem. Soc.* **2000**, *122*, 8685. Ni–FHF: Braun, T.; Foxon, S. P.; Perutz, R. N.; Walton, P. H. *Angew. Chem. Int. Ed.* **1999**, *38*, 3326.

(10) Selected examples with Cu(II) and Ni(II) as metal ions: (a) Manson, J. L.; Baldwin, A. G.; Scott, B. L.; Bendix, J.; Del Sesto, R. E.; Goddard, P. A.; Kohama, Y.; Tran, H. E.; Ghannadzadeh, S.; Singleton, J.; Lancaster, T.; Möller, J. S.; Blundell, S. J.; Pratt, F. L.; Zapf, V. S.; Kang, J.; Lee, C.; Whangbo, M.-H.; Baines, C. *Inorg. Chem.* **2012**, *51*, 7520. (b) Manson, J. L.; Carreiro, K. E.; Lapidus, S. H.; Stephens, P. W.; Goddard, P. A.; Del Sesto, R. E.; Bendix, J.; Ghannadzadeh, S.; Franke, I.; Singleton, J.; Lancaster, T.; Möller, J. S.; Baker, P. J.; Pratt, F. L.; Blundell, S. J.; Kang, J.; Lee, C.; Whangbo, M.-H. *Dalton Trans.* **2012**, *41*, 7235. (c) Manson, J. L.; Warter, M. L.; Schuelter, J. A.; Lancaster, T.; Steele, A. J.; Blundell, S. J.; Pratt, F. L.; Singleton, J.; Mc Donald, R. D.; Lee, C.; Whangbo, M.-H.; Plonczak, A. *Angew. Chem. Int. Ed.* **2011**, *50*, 1573.

(11) Levina, V. A.; Rossin, A.; Belkova, N. V.; Chierotti, M. R.; Epstein, L. M.; Filippov, O.; Gobetto, R.; Gonsalvi, L.; Lledós, A.; Shubina, E. S.; Zanobini, F.; Peruzzini, M. *Angew. Chem. Int. Ed.* **2011**, *50*, 1367.

(12) Rossin, A.; Peruzzini, M.; Zanobini, F. *Dalton Trans.* **2011**, *40*, 4447.

(13) (a) Miller, J.M. *Progress in Nuclear Magnetic Resonance Spectroscopy* 28, **1996**, 255. (b) Fernandes, R.G.; Ren, J.; De Camargo, A. S. S.; Hernandes, A. C. and Eckert, H. *J.Phys Chem. C* **2012**, *116*, 6434. (c) Martineau, C.; Fayon, F.; Suchomel, M. R.; Allix, M.; Massiot, D. and Taulelle, F. *Inorg. Chem.* **2011**, *50*, 2654.

(14) (a) Kovács, G.; Rossin, A.; Gonsalvi, L.; Lledós, A.; Peruzzini, M. *Organometallics* **2010**, *29*, 5121. (b) Rossin, A.; Gonsalvi, L.; Phillips, A. D.; Maresca, O.; Lledós, A.; Peruzzini, M. *Organometallics* **2007**, *26*, 3289. (c) Rossin, A.; Kovács, G.; Ujaque, G.; Lledós, A.; Joó, F. *Organometallics* **2006**, *25*, 5010.

(15) Frisch M. J. *et al.*, *Gaussian09, Revision A.02*, Gaussian Inc., Wallingford CT, **2009**.

(16) Zhao, Y.; Truhlar, D. G. *Theor. Chem. Account* **2008**, *120*, 215.

(17) Zhao, Y.; Truhlar, D. G. *Acc. Chem. Res.* **2008**, *41*, 157.

(18) (a) Andrae, D.; Haeussermann, U.; Dolg, M.; Stoll, H.; Preuss, H. *Theor. Chem. Acc.* **1990**, *77*, 123. (b) Dolg, M.; Wedig, U.; Stoll, H.; Preuss, H. *J. Chem. Phys.* **1987**, *86*, 866.

(19) Dunning T. H.; Hay P. J. *Modern Theoretical Chemistry*; H. F. Schaefer III Editor, 1976.

(20) Lynch, B. J.; Zhao, Y.; Truhlar, D. G.; *J. Phys. Chem. A* **2003**, *107*, 1384.

(21) (a) Höllwarth, A.; Böhme, M.; Dapprich, S.; Ehlers, A. W.; Gobbi, A.; Jonas, V.; Köhler, K. F.; Stegmann, R.; Veldkamp, A.; Frenking, G. *Chem. Phys. Lett.* **1993**, *208*, 237. (b) Ehlers, A.

W.; Böhme, M.; Dapprich, S.; Gobbi, A.; Höllwarth, A.; Jonas, V.; Köhler, K. F.; Stegmann, R.; Veldkamp, A.; Frenking, G. *Chem. Phys. Lett.* **1993**, *208*, 111.

(22) Marenich, A. V.; Cramer, C. J.; Truhlar, D. G. *J. Phys. Chem. B* **2009**, *113*, 6378.

(23) The static dielectric constant values of H_2O/THF mixtures at variable composition and at T = 298 K are taken from: Kinart, C. M.; Kinart, W. J. *Pol. J. Chem.* **1994**, *68*, 339.

(24) (a) Gancheff, J. S.; Kremer, C.; Denis, A.; Giorgi, C.; Bianchi, A. *Dalton Trans.* **2009**, 8257. (b) Kovács, G.; Schubert, G.; Joó, F.; Papai, I. *Organometallics* **2005**, *24*, 3059.

(25) Fukui, K. *Acc. Chem. Res.* **1981**, *14*, 363.

(26) The fluoride complex **2** is prepared through a chloride/fluoride exchange from the corresponding chloro complex (^{tBu}PCP)Ni(Cl) treated with TlF in MeOH [see reference (12)]. The Thallium(I) salt employed is highly hygroscopic; all the attempts made to dry it led to its decomposition. Small amounts of water are therefore unavoidable, and they are intrinsic to the preparative procedure employed.

(27) Gakh, Y. G.; Gakh, A. A.; Gronenborn, A. M. *Magn. Res. Chem.* **2000**, *38*, 551.

(28) Herzfeld, J. and Berger, A. E. *Chem. Phys.* **1980**, *73*, 6021.

(29) The $^{31}P\{^1H\}$ NMR chemical shift of the *aquo* species is strongly dependent on the counterion nature; in fact, the corresponding tetrafluoborate complex has δ_P = 69.0 ppm in the same solvent (THF-d_8): see reference (12). Formation of **5** is also confirmed by the appearance of its typical signals on the ^1H NMR spectrum. For a more detailed description, see reference (12).

(30) (a) Levina, V. A.; Filippov, O. A.; Gutsul, E. I.; Belkova, N. V.; Epstein, L. M.; Lledós, A.; Shubina, E. S. *J. Am. Chem. Soc.* **2010**, *132*, 11234. (b) Belkova, N. V.; Gutsul, E. I.; Filippov, O. A.; Levina, V. A.; Valayev, D. A.; Epstein, L. M.; Lledós, A.; Shubina, E. S. *J. Am. Chem. Soc.* **2006**, *128*, 3486.

(31) The exact position of the TS for this (rather complex) transformation could not be found, due to the simultaneous F^- dissociation and water coordination to the Ni(II) centre, joint to the hydrogen bonding network rearrangement that follows HF formation. All the attempts made to calculate it failed. Nonetheless, the PES scan along the d(Ni–F) reaction coordinate led to a maximum of the energy profile for d(Ni–F) = 2.5 Å, that can be reasonably considered very close to the real TS geometry. Therefore, the Gibbs energy of this point has been taken as an approximation of the real activation barrier.

(32) Grotthuss, C. J. T. *Ann. Chim.* **1806,** *58*, 54.

For Table of Contents use only

The reaction between the nickel(II) PCP pincer fluoride complex (^{tBu}PCP)Ni(F) and the tungsten(II) carbonyl hydride $CpW(H)(CO)_3$ leads to hydrogen fluoride formation, along with the bimetallic compound $[CpW(CO)_2(\mu\text{-}\kappa,C\text{:}\kappa,O\text{-}CO)\cdots Ni(^{tBu}PCP)]$. The fluoride-hydride interaction is not direct but water-mediated, different from that found for the related hydride-hydride pair. The process has been studied through multinuclear ^{19}F, ^{31}P and ^{1}H NMR spectroscopy combined with DFT calculations, at the M06//6-31+G(d,p) level of theory.